AIP | Journal of Applied Physics

Magneto-optical imaging using polarization modulation method

Takayuki Ishibashi, Zhihao Kuang, Shuta Yufune, Tetsuya Kawata, Masaru Oda, Toshiro Tani, Yasufumi Iimura, Katsuaki Sato, Yasushi Konishi, Kouich Akahane, Xiaoru Zhao, and Tetsuya Hasegawa

Citation: Journal of Applied Physics **100**, 093903 (2006); doi: 10.1063/1.2357699
View online: http://dx.doi.org/10.1063/1.2357699
View Table of Contents: http://scitation.aip.org/content/aip/journal/jap/100/9?ver=pdfcov
Published by the AIP Publishing

Magneto-optical imaging using polarization modulation method

Takayuki Ishibashi,[a] Zhihao Kuang, Shuta Yufune, Tetsuya Kawata, Masaru Oda, Toshiro Tani, Yasufumi Iimura, and Katsuaki Sato
Tokyo University of Agriculture and Technology, 2-24-16 Nakacho, Koganei, Tokyo 184-8588, Japan

Yasushi Konishi and Kouich Akahane
Neoark Corporation, 2-8-33 Wakamatsu-cho, Fuchu, Tokyo 183-0005, Japan

Xiaoru Zhao
National Institute for Materials Science, 1-1 Namiki Tsukuba, Ibaraki 305-0044, Japan

Tetsuya Hasegawa
The University of Tokyo, 7-3-1 Hongo, Bunkyo-ku, Tokyo 113-0033, Japan

(Received 5 April 2006; accepted 26 July 2006; published online 6 November 2006)

A magneto-optical (MO) microscope that uses the polarization modulation method has been developed for quantitative MO imaging. In this technique, images of MO rotation and ellipticity are reconstructed from three images for different polarization states; i.e., linear, right-circular, and left-circular polarization states. The three polarization states are generated either by rotating a quarter-wave plate or by changing the voltage applied to a liquid crystal modulator (LCM). Measurements are performed using a patterned thin film of Bi,Ga-substituted yttrium iron garnet prepared on a glass substrate. The values of MO rotation and ellipticity obtained from the images for several wavelengths between 450 and 650 nm are found to agree quantitatively with those obtained by an MO spectrometer. Hysteresis loops at any point of the image can be displayed by simply placing a pointer at the position. A real-time MO imaging with a rate of 1 frame/s is also achieved by using the LCM and a high-speed charge-coupled device camera. © *2006 American Institute of Physics*. [DOI: 10.1063/1.2357699]

I. INTRODUCTION

The magneto-optical (MO) microscope has become one of the most significant techniques for the observation of magnetic domain structures in magnetic materials. Recently, this technique has attracted a great deal of attention as a powerful tool for visualization of invisible phenomena, such as spin-injection current in semiconductors,[1,2] and magnetic flux in superconductors.[3–5] MO microscopes have technical advantages such as a short measurement time, simple instrumental setup compared to other imaging techniques, such as the magnetic force microscope (MFM),[6] the superconducting quantum interference device (SQUID) microscope,[7] and the Hall-probe microscope.[8] However, MO imaging using a conventional crossed-polarizer method has drawbacks such as difficulty in the quantitative evaluation of the MO effect and difficulty in the measurement of inhomogeneous materials and the darkness of the obtained images. For example, in the case of Faraday measurement, quantitative evaluation requires calibration of the intensity of the incident polarized light beam I_0 for each measurement, since the light intensity depends on the absorption coefficient γ and the thickness d of the sample, as given by $I=I_0 \exp(-\gamma d)\sin^2(\theta_F+\Delta\alpha)$, where θ_F denotes the Faraday rotation and $\Delta\alpha$ an angle shift from the crossed (90°) alignment between the polarizer and the analyzer. It is therefore difficult to measure samples with inhomogeneous transmission or reflectivity. Moreover, with this method, simultaneous evaluation of the rotation and the ellipticity is not possible without changing the setup.

In order to solve the above-mentioned problems, we have proposed a MO imaging technique using a polarization modulation technique, which has been widely used for MO spectroscopic measurement.[9,10] In the MO imaging using the polarization modulation method, quantitative images of MO rotation and ellipticity can easily be obtained using three images taken with three different polarization states, i.e., linearly polarized (LP) light, right-circularly polarized (RCP) light, and left-circularly polarized (LCP) light.[11,12] However, there is a drawback in that at least several tens of seconds are required for measurement because of a procedure to modulate optical polarization states by mechanical rotation of a quarter-wave plate. To overcome this drawback, we used a liquid crystal modulator (LCM), so that the optical polarization state can be changed by simply changing the ac voltage applied to the device. Although MO imaging using a liquid crystal device for accurate MO imaging has been reported already by Zhu *et al.*,[13] the method requires significant time because several calculations, including Fourier analysis, must be performed. For fast MO imaging, Wijngaarden *et al.* succeeded in the measurement of angle of rotation using a Faraday rotator.[14] However, in this case it is impossible to evaluate the rotation and the ellipticity simultaneously.

[a]Electronic mail: bashi@cc.tuat.ac.jp

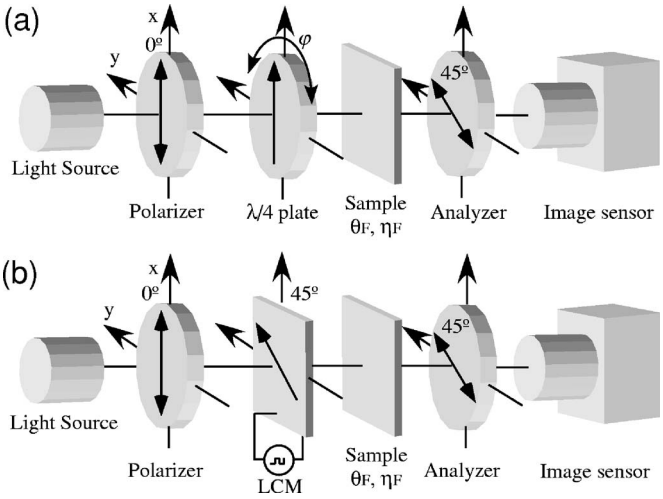

FIG. 1. Schematic drawing of optical setups for MO imaging using (a) a quarter-wave plate and (b) a liquid crystal modulator.

In the present article, we describe the physical explanation of the MO microscope utilizing a polarization modulation technique, and we report experimental results for both quantitative and real time measurements.

II. POLARIZATION MODULATION METHOD FOR MO IMAGING

The polarization modulation method was originally developed in the late 1960s for magnetic circular dichroism (MCD) measurements[15,16] and was later extended to MO rotation spectroscopy.[9,10] The MO measurement system consists of a polarizer, a photoelastic modulator (PEM), an analyzer, and a photodetector. The PEM typically cycles alternately between three polarization states at 50 kHz: left-circular polarization (LCP) → a linear polarization (LP) → right-circular polarization (RCP) → LP. If the sample has no optical activity (no change in the polarization state), the intensity of light after the analyzer does not change. The light intensity changes at the doubled frequency (100 kHz) if the sample has a MO rotation, whereas it changes at the same frequency (50 kHz) if the sample has a MO ellipticity. For this purpose, the lock-in detection method is employed for MO measurements.

On the other hand, in the case of MO imaging, lock-in detection cannot be employed because image sensors, such as charge-coupled device (CCD) cameras, cannot respond to the modulation frequency of the PEM. Rather than lock-in detection, we take the difference between two images corresponding to different polarization states by using an image-processing technique, which is equivalent to the PEM lock-in method. To generate different polarization states, we use either a mechanically rotating quarter-wave plate or a liquid crystal modulator (LCM). Schematic drawings of MO microscopes using a quarter-wave plate and a LCM are shown in Figs. 1(a) and 1(b), respectively.

In the following, we explain the principle of the polarization-modulation MO imaging technique in terms of the Jones matrix method. Each optical component shown in Fig. 1 is expressed in terms of a Jones matrix. The matrix of the polarizer with its optic axis parallel to the vertical axis (x) is expressed by

$$\mathbf{P} = \begin{pmatrix} 1 & 0 \\ 0 & 0 \end{pmatrix}. \tag{1}$$

The phase shifter of retardation δ with optic axis making an angle ϕ with the vertical (x) axis is expressed as

$$\mathbf{J} = \begin{pmatrix} e^{i\delta/2}\cos^2\phi + e^{-i\delta/2}\sin^2\phi & (e^{i\delta/2} - e^{-i\delta/2})\sin\phi\cos\phi \\ (e^{i\delta/2} - e^{-i\delta/2})\sin\phi\cos\phi & e^{i\delta/2}\sin^2\phi + e^{-i\delta/2}\cos^2\phi \end{pmatrix}. \tag{2a}$$

Consequently, the matrix of a rotating quarter-wave plate $(\delta = \pi/2)$ with angle ϕ is denoted by

$$\mathbf{J}_Q = \frac{1}{\sqrt{2}}\begin{pmatrix} 1 + i\cos 2\phi & i\sin 2\phi \\ i\sin 2\phi & 1 - i\cos 2\phi \end{pmatrix}, \tag{2b}$$

where LP, RCP, and LCP correspond to $\phi = 0$, $\pi/4$, and $-\pi/4$, respectively. On the other hand, the matrix for the LCM in which retardation δ can be controlled by an applied voltage is given by

$$\mathbf{J}_L = \frac{1}{2}\begin{pmatrix} e^{i\delta/2} + e^{-i\delta/2} & e^{i\delta/2} - e^{-i\delta/2} \\ e^{i\delta/2} - e^{-i\delta/2} & e^{i\delta/2} + e^{-i\delta/2} \end{pmatrix}, \tag{2c}$$

where LP, RCP, and LCP correspond to $\delta = 0$, $\pi/2$, and $-\pi/2$, respectively. For a Faraday configuration shown in Fig. 1, the matrix of a sample having Faraday rotation θ_F and Faraday ellipticity η_F is expressed by

$$\mathbf{S} = \begin{pmatrix} \cos\theta_F + i\eta_F\sin\theta_F & -\sin\theta_F + i\eta_F\cos\theta_F \\ \sin\theta_F - i\eta_F\cos\theta_F & \cos\theta_F + i\eta_F\sin\theta_F \end{pmatrix}. \tag{3}$$

In the case of a Kerr configuration, the matrix is expressed in the same form by replacing the θ_F and η_F with Kerr rotation θ_K and Kerr ellipticity η_K. The analyzer with an optical axis of 45° is

$$\mathbf{A} = \frac{1}{2}\begin{pmatrix} 1 & 1 \\ 1 & 1 \end{pmatrix}. \tag{4}$$

Using these matrices, an output signal $\mathbf{E}_2$ using the quarter-wave plate can be calculated as follows:

$$\mathbf{E}_2 = \mathbf{ASJ}_Q\mathbf{PE}_1 = \frac{1}{2\sqrt{2}}\begin{pmatrix}1 & 1\\ 1 & 1\end{pmatrix}\begin{pmatrix}\cos\theta_F + i\eta_F\sin\theta_F & -\sin\theta_F + i\eta_F\cos\theta_F\\ \sin\theta_F - i\eta_F\cos\theta_F & \cos\theta_F + i\eta_F\sin\theta_F\end{pmatrix}\times\begin{pmatrix}1 + i\cos 2\phi & i\sin 2\phi\\ i\sin 2\phi & 1 - i\cos 2\phi\end{pmatrix}\begin{pmatrix}1 & 0\\ 0 & 0\end{pmatrix}$$
$$\times\begin{pmatrix}E_x\\ E_y\end{pmatrix} = \frac{1}{2\sqrt{2}}\begin{pmatrix}\cos\theta_F + \sin\theta_F - \eta_F(\sin(2\phi+\theta_F) - \cos(2\phi+\theta_F))\\ +i(\cos(2\phi+\theta_F) + \sin(2\phi+\theta_F) + \eta_F(\sin\theta_F - \cos\theta_F))\\ \cos\theta_F + \sin\theta_F - \eta_F(\sin(2\phi+\theta_F) - \cos(2\varphi+\theta_F))\\ +i(\cos(2\phi+\theta_F) + \sin(2\phi+\theta_F) + \eta_F(\sin\theta_F - \cos\theta_F))\end{pmatrix}E, \tag{5}$$

where $\mathbf{E}_1=(E_x,E_y)$ is an input light. Consequently, the intensity measured at the detector is the square of the absolute value of $\mathbf{E}_2$ as a function of θ_F, η_F, and ϕ,

$$I(\theta_F,\eta_F,\phi) = ((\cos\theta_F + \sin\theta_F - \eta_F(\sin(2\phi+\theta_F) - \cos(2\phi+\theta_F)))^2 + (\cos(2\varphi+\theta_F) + \sin(2\phi+\theta_F) + \eta_F(\sin\theta_F - \cos\theta_F))^2)|E_x|^2/4. \tag{6}$$

In the case of the LCM, the output signal $\mathbf{E}_2$ and the intensity can also be calculated by the same procedure using the matrix $\mathbf{J}_L$ for the LCM rather than the matrix $\mathbf{J}_Q$. Thus, the intensity of the light is expressed as a function of θ_F, η_F, and δ as follows:

$$I(\theta_F,\eta_F,\delta) = |\sin\theta_F - i\eta_F\cos\theta_F + e^{i\delta}(\cos\theta_F + i\eta_F\sin\theta_F)|^2|E_x|^2/2. \tag{7}$$

For both cases, images of Faraday rotation θ_F and ellipticity η_F can be reconstructed using three images for different polarization states, LP, RCP, and LCP, as follows:

$$\theta_F = \frac{1}{2}\sin^{-1}\frac{2I_{\mathrm{LP}} - (I_{\mathrm{RCP}} + I_{\mathrm{LCP}})}{(1-\eta_F^2)|E_x^2|}, \tag{8}$$

$$\eta_F = \frac{I_{\mathrm{RCP}} - I_{\mathrm{LCP}}}{2|E_x^2|}, \tag{9}$$

where I_{LP}, I_{RCP}, and I_{LCP} are the intensities at the detector obtained with LP, RCP, and LCP, respectively. For small values of θ_F and η_F of less than a few degrees, Eqs. (8) and (9) can be reduced to simple expressions (10) and (11) by replacing $|E_x|^2$ with $(I_{\mathrm{LCP}}+I_{\mathrm{RCP}})$ as follows:

$$\theta_F = \frac{2I_{\mathrm{LP}} - (I_{\mathrm{RCP}} + I_{\mathrm{LCP}})}{2(1-\eta_F^2)(I_{\mathrm{RCP}} + I_{\mathrm{LCP}})}, \tag{10}$$

$$\eta_F = \frac{I_{\mathrm{RCP}} - I_{\mathrm{LCP}}}{2(I_{\mathrm{RCP}} + I_{\mathrm{LCP}})}. \tag{11}$$

Note that, for large values of θ_F and η_F, Eqs. (10) and (11) may include large errors. For example, the error is 35% in θ_F and 22% in η_F for $\theta_F=30°$ and $\eta_F=30°$, whereas these errors are less than 0.1% for $\theta_F=1°$ and $\eta_F=1°$.

In this system, light intensities I_{LP}, I_{LCP}, and I_{RCP} are approximately 25% of the input light intensity $I_{\mathrm{IN}}=|\mathbf{E}_1|^2$ if a sample absorption is neglected, whereas the light intensity is no more than 1% of I_{IN} in the crossed-polarizer technique. In the latter technique the angle of the analyzer α is set at an angle that differs slightly (approximately 5°) from the extinction point, which leads to a poor intensity, for example, 0.76% of I_{IN} for $\alpha=5°$. This means that the proposed technique requires less sensitivity for an image sensor. In addition, the brightness of images is crucial for a real-time MO imaging, because the higher the intensity of the image the shorter the exposure time.

III. MO IMAGING SYSTEM

Figure 2 shows a schematic drawing of the developed MO imaging system. In order to utilize the optical modulation technique described in the previous section, a polarizer, a liquid crystal modulator, and an analyzer were installed, and objective lenses (Mitsutoyo, G Plan APO ×10, ×50) were employed. Digital images of 640× 480 pixels were captured by a high-speed CCD camera (Hamamatsu, C9300–201) with a 12-bit A/D converter, which can directly transfer 160 digital images/s to RAM in the computer. A green LED with a central wavelength of 525 nm or a halogen lamp with an interference filter was used as a light source. Although Fig. 2 shows a Kerr configuration, a Faraday configuration is also possible by moving the light source, the polarizer, and the LCM behind the magnet.

The LCM used in the present work was prepared with a commercially available liquid crystal (ZLI-4792) and ITO-coated glass plates. The retardation was varied by the application of ac voltage of 0–10 V with a frequency of approximately 100 Hz to the LCM in this experiment. In order to find the voltages for the LCP, the LP, the RCP, the extinction

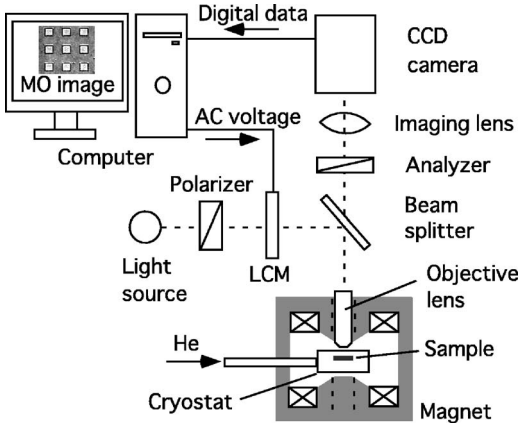

FIG. 2. A schematic drawing of the MO imaging system used in the present study.

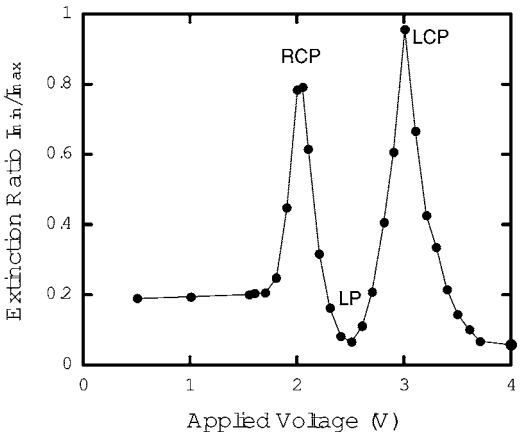

FIG. 3. The extinction ratio between the I_{min} and the I_{max} depending on an ac voltage applied to the LCM.

ratio, i.e., the ratio of the minimum intensity I_{min} to the maximum intensity I_{max}, of the output light, was measured as shown in Fig. 3. The maxima and the minimum in Fig. 3 correspond to the circularly polarized lights and the linearly polarized light, respectively, from which voltages to provide RCP, LP, and LCP are determined as 2.0, 2.5, and 3.0 V, respectively. This feature means that an optical retardation can be modulated quickly by changing the ac voltage applied to the LCM. Although the handmade LCM used in the present study responded in 0.2 s, a faster LCM with a switching time of less than 10 ms is also available. Magneto-optical images are obtained by controlling the LCM and the CCD camera simultaneously using software developed in the present study. Real-time measurement using this technique is discussed in the next section.

IV. MO IMAGES OF PATTERNED Bi,Ga:YIG FILMS

Bi, Ga-substituted yttrium iron garnet (YIG) thin film showing a perpendicular magnetization prepared by a metal-organic decomposition method[17] was used as a sample. In order to investigate the resolution of the magneto-optical contrast, the garnet thin film was patterned into square dot arrays by a photolithography. Each dot has an area of 50 $\times$ 50 μm and a thickness of 200 nm, and the dot separation is 50 μm. The Faraday images shown in this section were measured using a quarter-wave plate as a polarization modulator,[12] and a halogen lamp and interference filters were employed so that light with a wavelength between 450 and 650 nm could be used.

Figure 4 shows images of the Faraday rotation (a) and (b), and the Faraday ellipticity (c) and (d), of the garnet dot structure measured by using a quarter-wave plate at the wavelength of 500 nm. These images are reconstructed from three images taken with LP, LCP, and RCP by applying Eqs. (10) and (11) at each pixel point. Upper images [Figs. 4(a) and 4(c)] and lower images were measured for opposite remanent states after magnetizing toward opposite directions by the saturating field. A reversal of the magnetic contrast between the glass and the garnet portions is clearly observed, corresponding to a magnetization reversal. In addition to the magnetic contrast, quantitative values of θ_F and η_F can be

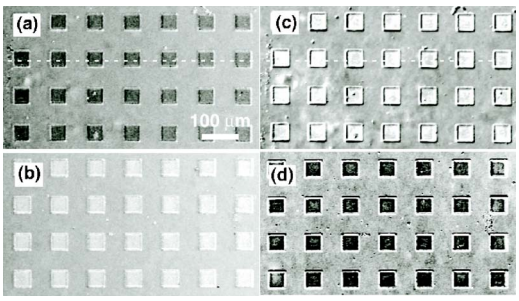

FIG. 4. (a) and (b) are Faraday rotation images and (c) and (d) are Faraday ellipticity images with opposite remanent states. A rotation image and an ellipticity image, (a) and (c) or (b) and (d), were obtained from same images for LP, LCP, and RCP.

obtained at any pixel on the image. Therefore, the present technique provides a quantitative magnetic contrast even in inhomogeneous samples consisting of different portions with different transmittance, for which the conventional crossed-polarizer method fails to provide quantitative MO values, because it measures contrast as the difference in optical intensities.

The cross-sectional plots of the Faraday rotation θ_F and ellipticity η_F along the dotted lines in Fig. 4 are shown in Fig. 5. The values of θ_F and η_F in the garnet dots are determined to be 0.5° and 0.3°, respectively. The results measured for a wavelength of 450–650 nm are plotted in Fig. 6 together with solid lines showing the data for a continuous film as measured by an MO spectrometer.[10] As observed in the figure, MO values measured by the MO microscope are found to show a remarkable agreement with those measured by the MO spectrometer.

Since most magnetic materials are not transparent, measurement of the Kerr effect is important for practical use. To measure images of Bi,Ga:YIG with a Kerr configuration, the sample was placed on a Si wafer, because the sample is relatively transparent for a wavelength of 525 nm and the sample holder does not maintain the polarization state of the light. Figure 7 shows the magnified rotation images of the garnet dot pattern measured using the LCM with various magnetic fields. The objective lens used for this measurement is a Mitsutoyo G Plan APO ×50, with NA=0.5. The magnetic contrast between the garnet and the glass is also

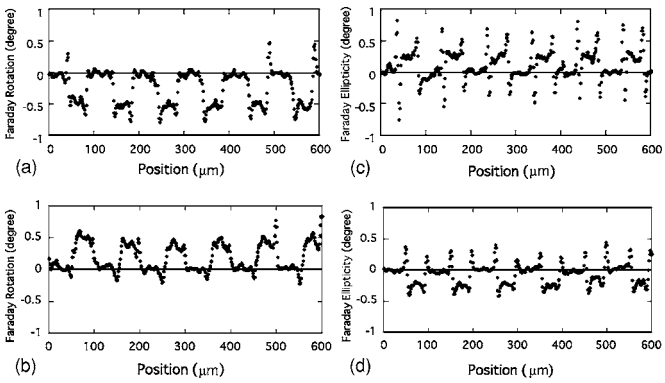

FIG. 5. Line profiles of the image of Faraday rotation shown in Fig. 4. Spikelike noise observed at the edge of the pattern is due to depolarization of the light by the edge.

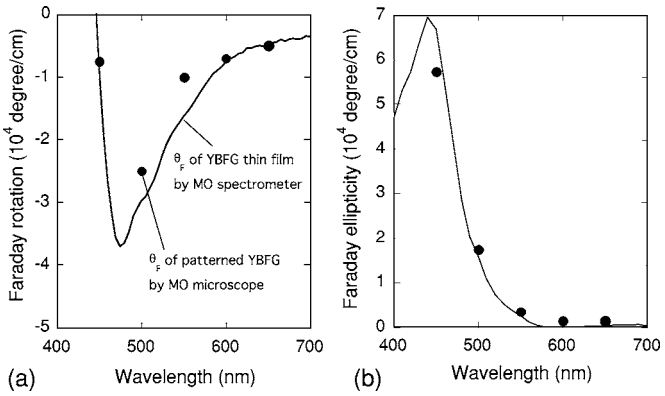

FIG. 6. (a) Faraday rotation and (b) Faraday ellipticity spectra. Solid curves show spectra measured by a conventional spectrometer for the continuous film, and dots show data measured by the MO microscope.

clearly obtained, and magnetic domains of approximately 1 μm in diameter are clearly resolved. Figure 8 shows an enlarged image of the region indicated by the square in Fig. 7 as well as a line profile of the magnetic domain. A spatial resolution in these images was estimated to be 0.5 μm, which is consistent with that expected from the value of NA of the objective lens. This result shows that the polarization modulation method does not degrade the spatial resolution of MO images.

The sensitivity of MO images is limited primarily by the shot noise generated in the CCD device. Therefore, we carried out two types of averaging procedures in order to improve the signal-to-noise ratio. The first procedure is an averaging of the intensity by repeated data accumulation in each pixel, and the other procedure is an averaging of 9 pixels including 8 pixels surrounding the pixel in question. The sensitivity was estimated by measuring a noise in MO images of a Si wafer. Averaging of 100 and 1000 images gives us standard deviation of 0.008° and 0.005° for the angle of rotation.

Once MO images are acquired for a sequence of magnetic field swinging between negative and positive magnetic saturation, hysteresis curves at any pixel point can be visualized. Figure 9 shows the magnetic field dependences of rotation for a garnet dot and a glass substrate, shown in the inset of Fig. 9. This measurement was performed by a Kerr

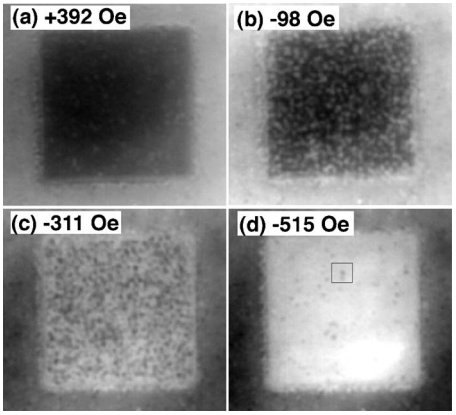

FIG. 7. Kerr rotation images of the patterned Bi,Ga:YIG on glass substrate with different magnetic fields.

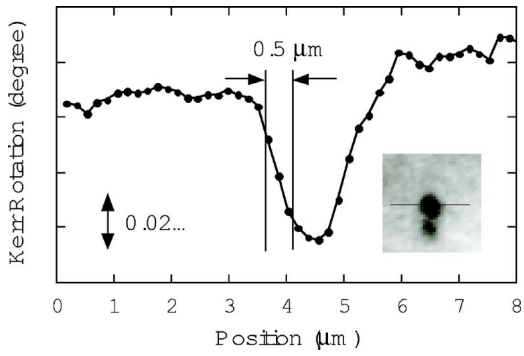

FIG. 8. The enlarged image and the line profile of Kerr rotation of the small magnetic domain.

configuration using a light of wavelength 500 nm by a halogen lamp with an interference filter. A clear hysteresis loop was observed for the garnet pattern, while no signal was obtained for the glass substrate.

Finally, we describe the real-time measurement. Although the present technique is more complicated than the conventional crossed-polarizer technique, a real-time measurement becomes possible by utilizing the LCM and the software developed in the present study. Figure 10 shows an example of the real-time measurement of Kerr rotation images of the patterned garnet dot. In order to increase the frame rate, we simplified Eq. (10) assuming $I_{\mathrm{RCP}} \approx I_{\mathrm{LCP}}$ as expressed by

$$\theta_F = \frac{I_{\mathrm{LP}} - I_{\mathrm{RCP}}}{2I_{\mathrm{RCP}}}. \tag{12}$$

In this measurement, optical images were captured with an exposure time of 20 ms, and 10 images were averaged for each circular polarization image in order to reduce shot noise. As a result, MO images could be displayed at a rate of approximately 1 frame/s. We hope to improve the frame rate to the video rate by appropriate selection of a fast-response LCM.

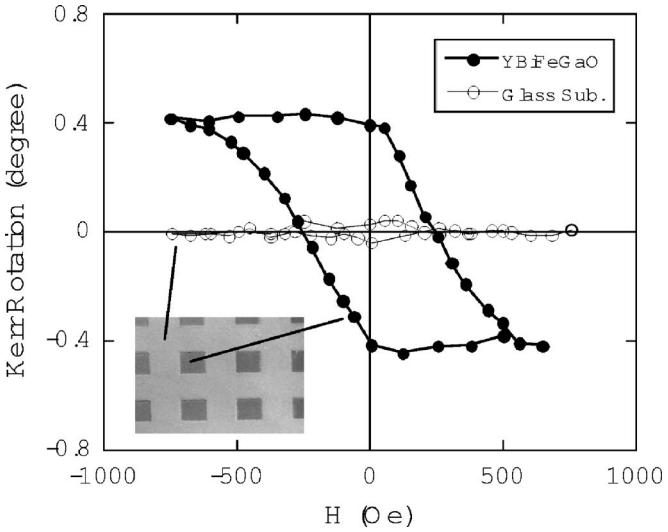

FIG. 9. Magnetic field dependences of the Kerr rotation for the garnet dot and the glass substrate.

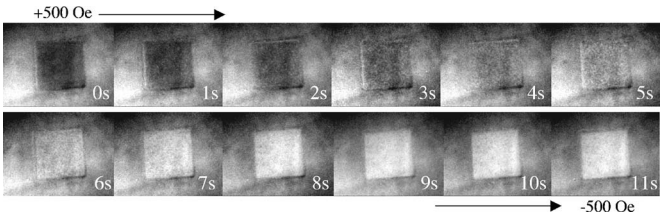

FIG. 10. MO images measured with various magnetic fields. The frame rate was 1 s.

V. CONCLUSIONS

We have developed a MO microscope using an optical modulation technique. In addition to the clear magnetic contrast obtained for patterned Bi,Ga-substituted YIG dot structures having inhomogeneous transmittance and reflectivity, quantitative measurement was demonstrated for wavelengths between 450 and 650 nm. Hysteresis measurement in the MO imaging with spatial resolution of 0.5 μm was also demonstrated. By carrying out averaging procedure, the resolution in the rotation angle was estimated to be better than 0.01°, and using the LCM, a frame rate of 1 frame/s was achieved.

ACKNOWLEDGMENTS

This study was supported in part by the 21st COE Project "Future Nano Materials" of TUAT and Grant-in-Aid for Scientific Research (Nos. 14655151 and 16360003) from the Japan Society for the Promotion of Science.

[1] S. A. Crooker, M. Furis, X. Lou, C. Adelmann, D. L. Smith, C. J. Palmstrøm, and P. A. Crowell, Science **309**, 2191 (2005).
[2] M. Yamanouchi, D. Chiba, F. Matsukura, and H. Ohno, Nature **428**, 539 (2004).
[3] S. Gotoh, N. Koshizuka, M. Yoshida, M. Murakami, and S. Tanaka, Jpn. J. Appl. Phys., Part 2 **29**, L1083 (1990).
[4] M. V. Indenbom, N. N. Kolesnikov, M. P. Kulakov, I. G. Naumenko, V. I. Nikitenko, A. A. Polyanskii, N. F. Vershinin, and V. K. V. Vlasov, Physica C **166**, 486 (1990).
[5] P. E. Goa, H. Hauglin, A. A. F. Olsen, D. Shantsev, and T. H. Johansen, Appl. Phys. Lett. **82**, 79 (2003).
[6] Y. Martin, D. Rugar, and H. K. Wickramasinghe, Appl. Phys. Lett. **52**, 244 (1988).
[7] J. R. Kirtley, M. B. Ketchen, K. G. Stawiasz, J. Z. Sun, W. J. Gallagher, S. H. Blanton, and S. J. Wind, Appl. Phys. Lett. **66**, 1138 (1995).
[8] A. M. Chang, H. D. Hallen, L. Harriott, H. F. Hess, H. L. Kao, J. Kwo, R. E. Miller, R. Wolfe, J. van der Ziel, and T. Y. Chang, Appl. Phys. Lett. **61**, 1974 (1992).
[9] K. Sato, Jpn. J. Appl. Phys. **20**, 2403 (1981).
[10] K. Sato, H. Hongu, H. Ikekame, Y. Tosaka, M. Watanabe, K. Takanashi, and H. Fujimori, Jpn. J. Appl. Phys., Part 1 **32**, 989 (1993).
[11] X. R. Zhao, N. Okazaki, Y. Konishi, K. Akahane, Z. Kuang, T. Ishibashi, K. Sato, H. Koinuma, and T. Hasegawa, Appl. Surf. Sci. **223**, 73 (2004).
[12] T. Ishibashi, Z. Kuang, Y. Konishi, K. Akahane, X. R. Zhao, T. Hasegawa, and K. Sato, Plann. High. Educ. **4**, 278 (2004).
[13] X. S. Zhu, H. B. Zhao, P. Zhou, G. Q. Xia, H. Y. You, R. J. Zhang, J. Li, S. Y. Wang, W. M. Ni, and L. Y. Chen, Rev. Sci. Instrum. **74**, 4718 (2003).
[14] R. J. Wijngaarden, K. Heeck, M. Welling, R. Limburg, and M. Pannetier, Rev. Sci. Instrum. **72**, 2661 (2001).
[15] S. N. Jasperson and S. E. Schnatterly, Rev. Sci. Instrum. **40**, 761 (1969).
[16] R. A. Shatwell and A. J. McCaffery, Phys. Rev. B **12**, 3815 (1975).
[17] T. Ishibashi, A. Mizusawa, M. Nagai, S. Shimizu, and K. Sato, J. Appl. Phys. **97**, 013516 (2005).